

Density change effects on crystal growth from the melt

Massimo Conti

*Dipartimento di Matematica e Fisica, Università di Camerino, and Istituto Nazionale di Fisica della Materia,
Via Madonna delle Carceri, I-62032, Camerino, Italy*

(Received 21 March 2001; published 17 October 2001)

When a crystal grows from its undercooled melt the local density changes, driving a convective flow in the liquid phase. Then, the purely diffusional description of the process ceases to be satisfactory. Moreover, the dynamic pressure associated with the flow field may affect the melting temperature (and the effective undercooling) of the system. Both these effects have been addressed in recent experimental work. In the present study we derive a thermodynamically consistent phase-field model that accounts for the density change effects in the solidification of a pure substance. Starting from a thermodynamic potential that includes squared gradient terms for both the order parameter and the density, the field equations are derived assuming positive local entropy production. The model is numerically solved in one dimension to show deviations from the classic phase-field description of the same phenomenon.

DOI: 10.1103/PhysRevE.64.051601

PACS number(s): 81.15.Lm, 64.70.Dv, 81.30.Bx, 05.70.Np

I. INTRODUCTION

Solidification from an undercooled melt is accompanied by a local change of density. The solid is generally denser than the liquid. The change is typically a few percent for simple metals. In some cases (silicon, bismuth, water) the reverse is observed, and the liquid expands upon freezing. The change of density during the phase transition causes a flow in the liquid towards the solid-liquid interface or away from it, depending on the sign of the density effect. This mass advection in turn carries heat. Consequently, even in absence of natural convection in the liquid phase, the aspect of the growth process that involves pure diffusion ceases to be satisfactory and must be coupled with an accurate description of hydrodynamic phenomena. This point emerged in the interpretation of some recent experiments conducted by Glicksman and co-workers aboard the space shuttle [1]. In a microgravity environment, where natural convection was suppressed, these authors studied the growth of a free dendrite. The experimental data show a departure from the predictions of the Ivantsov diffusional theory [2]. A careful re-examination of the data, based on a refinement of the Ivantsov approach [3] to incorporate flow effects, showed that, apart from some finite size effects, any inconsistency could be removed taking into account the additional heat transfer due to the advection mechanism [4].

A further effect due to the density change (and to the consequent flow field) results from the dynamic pressure drop across the melt. At large growth rates the pressure increase (or decrease) at the interface may significantly alter the equilibrium melting temperature. This point has been previously considered by Horvay [5], who studied the tension field created by a spherical nucleus freezing into an infinite undercooled melt of lower density. In his study, based on the free boundary approach, the liquid phase is treated as an incompressible inviscid fluid and the transition temperature is viewed as affected by both the curvature of the nucleus and the hydrodynamic pressure due to the flow. A similar analysis was subsequently conducted by Charach and Rubinstein [6] for the growth of a planar interface. Both

these studies showed that, due to the effects of the pressure field, some inconsistencies of the classic Stefan formulation of the problem could be removed and the interface velocity is free of singularities during the entire freezing process. It is worth noting that a shift of the equilibrium melting temperature induced through a static pressure field has been recently proposed as a method to control the growth dynamics of the solidification process [7].

The theoretical description of density effects in solidification has been generally based on the free boundary formulation of the problem, coupled with proper interface boundary conditions. With respect to the classic Stefan problem, the latter must incorporate additional constraints for the mass and momentum conservation. A more stimulating approach could be based on the phase-field model (PFM), which replaces the sharp solid-liquid interface with a diffuse interface. In this model the phase of the system at each point is characterized by an order parameter $\phi(\mathbf{x}, t)$ that assumes constant values in the bulk phases and varies continuously in the interface region. A suitable thermodynamic potential is then constructed, that depends on ϕ as well as on the other relevant thermodynamic variables; squared gradient terms account for the energy cost of the interface. The extremization of the functional in respect to these variables results in the dynamic equations for the process. Several studies both analytical [8–13] and numerical [14,15] established on a firm basis the notion that the phase-field model for a pure substance, in the limit of a vanishingly small interface width, reduces to the sharp-interface diffusional equations, incorporating in a natural fashion the Gibbs-Thomson effect as well as the kinetic undercooling of the moving interface. Moreover, the extension of the PFM to the solidification of binary alloys [16–22], accounts for non-equilibrium effects as solute trapping, and was able to interpret complex phenomena as the formation of solute bands in solidification far from equilibrium.

Caginalp and Jones [23,24] were the first to extend the phase-field model to incorporate flow effects, within the context of a unified and consistent derivation. They obtained a system of differential equations for the variables tempera-

ture, order parameter, fluid velocity, density, and pressure. In the momentum equation, capillary and viscosity effects were neglected. An asymptotic analysis led to a new interface relation, showing that the front velocity in the kinetic undercooling term should be replaced by the front velocity minus the normal fluid velocity.

In a subsequent study, Oxtoby [25] introduced a grand canonical potential in which, besides the nonconserved phase field, also the local density is regarded as a (conserved) order parameter. The dynamic equation for the growth rate results from the extremization of the potential in respect to the phase field, and the Navier-Stokes equation is written in the interfacial region using an expression for the capillary stress tensor that is derived resorting to density functional arguments. Then, the coupled problem to determine the growth rate and the flow field is stated through the above equations and the mass conservation condition. Steady state solutions of the model, obtained in isothermal conditions, put in evidence the role of sound modes in density transport.

In the present paper we present a phase-field model that accounts for the change of density in the solidification process. Following a scheme suggested by Charach [26], the entropy production equation, coupled with the balance of mass, momentum, and energy, is used to derive governing equations of the model that drive the system towards equilibrium. In this sense the model extends the approach of Antanovskii [27] and Anderson, McFadden and Wheeler [28], incorporating the nonconserved order parameter and allowing one to treat solid-liquid phase transitions. Several ideas come also from the analysis of Yang, Fleming, and Gibbs [29] for a liquid-gas interface of a one component system. The scalar part of the entropy production fixes the dynamic equation for the structural order parameter; the vector contribution results in the classic Fourier expression for the heat flux. A third term, of tensorial character, allows to find an expression for the stress tensor, starting from the assumption that this contribution is only due to viscous dissipation. This form of the capillary tensor satisfies the Euler-Lagrange conditions for the grand canonical potential when the system is in equilibrium.

The equations of the model have been solved numerically in one dimension, to study the coupled effects of the thermal, mechanical, and chemical relaxation on the growth process. As solidification starts, the sudden contraction of the liquid in front of the interface originates a pressure (and density) wave that propagates into the sample. The results of our simulations show that this phenomenon, as well as the dynamics of the interface advancement, of the advected flow field and the stress field is properly described. For isothermal growth we found that in a wide range of temperatures the growth rate increases almost linearly with increasing the interface undercooling. When the thermal field is allowed to relax, we observe that the purely diffusive dynamics of the process is only slightly affected by the convective heat transfer. This point merits further investigation. At present we cannot predict whether these small deviations could result in more remarkable effects when different materials or geometries are considered.

The paper is organized as follows. In Sec. II the equilib-

rium of a two-phase system will be analyzed. The dynamic equations of the model will be derived in Sec. III, using the concepts of the extended irreversible thermodynamics. In Sec. IV we present the scheme for the numerical solution of the model, and in Sec. V the results of the numerical simulations will be discussed. The conclusions will follow in Sec. VI.

II. EQUILIBRIUM OF A TWO-PHASE SYSTEM

A. A closed system

Let us first consider a closed solid-liquid system in equilibrium at fixed temperature T and volume V . The local state of the system is characterized by a coarse grained density $\rho(\mathbf{x}, t)$ and a nonconserved order parameter $\phi(\mathbf{x}, t)$. We postulate a generalized Helmholtz free energy density of the form

$$\psi'(\rho, \phi, T, \nabla \rho, \nabla \phi) = \psi(\rho, \phi, T) + \frac{1}{2} \delta_F^2 (\nabla \rho)^2 + \frac{1}{2} \epsilon_F^2 (\nabla \phi)^2, \quad (1)$$

where $\psi(\rho, \phi, T)$ is the bulk free energy density and the gradient terms account for nonlocal contributions in the interfacial region. We assume that ϵ_F and δ_F depend only on temperature. We wish to derive the equations for the spatial variation of the density ρ and the phase field ϕ . As the whole system is closed, minimizing the total Helmholtz free energy gives

$$\delta(F - \mu_0 M) = \delta \int (\psi' - \mu_0 \rho) dv = 0, \quad (2)$$

where μ_0 is a Lagrange multiplier; the corresponding Euler-Lagrange equations read:

$$\delta_F^2 \nabla^2 \rho - \frac{\partial w}{\partial \rho} = 0, \quad \epsilon_F^2 \nabla^2 \phi - \frac{\partial w}{\partial \phi} = 0, \quad (3)$$

where

$$w(\rho, \phi, T) = \psi(\rho(\mathbf{r}), \phi(\mathbf{r}), T) - \rho(\mathbf{r}) \mu_0(T). \quad (4)$$

Let us consider the planar one-dimensional case and assign $z=0$ at the position of the Gibbs dividing plane (phase interface). In the bulk phases, recalling that the chemical potential is given by $\mu = \partial \psi / \partial \rho$, Eqs. (4) and (3) reduce to

$$\mu_s = \mu_l = \mu_0; \quad \left(\frac{\partial \psi}{\partial \phi} \right)_{\phi=\phi_s} = \left(\frac{\partial \psi}{\partial \phi} \right)_{\phi=\phi_l} = 0, \quad (5)$$

where the subscripts s, l indicate the physical properties in the bulk solid and liquid phases, respectively. Multiplying the first of Eqs. (3) by ρ_z and the second by ϕ_z and adding them together, we obtain, through simple integration

$$\frac{1}{2} (\delta_F^2 \rho_z^2 + \epsilon_F^2 \phi_z^2) + \rho(z) \mu_0(T) - \psi(\rho(z), \phi(z), T) = P_0(T). \quad (6)$$

Here $P_0(T)$ is clearly the coexistence pressure at temperature T , since in the bulk, where $\rho_z, \phi_z = 0$ it reduces to the usual expression $p = \mu\rho - \psi$. Equations (5) and (6) define the chemical and mechanical equilibrium of the two-phase system. Equations (1) and (6) allow to find a simple expression for the surface tension. We rewrite Eq. (6) as

$$(\delta_F^2 \rho_z^2 + \epsilon_F^2 \phi_z^2) + \rho(z)\mu_0(T) - \psi'(\rho(z), \phi(z), T) = P_0(T). \quad (7)$$

When Eq. (7) is integrated over the total volume of the system (from $-L$ far in the solid to $+L$ far into the liquid), it can be written as

$$F = \mu_0 M - P_0 V + \gamma A, \quad (8)$$

where A is the system cross section and the surface tension γ is given by

$$\gamma = \int_{-L}^{+L} (\delta_F^2 \rho_z^2 + \epsilon_F^2 \phi_z^2) dz. \quad (9)$$

This result extends to a solid-liquid phase transition with density change well known results obtained either for fluid-fluid interfaces or for solidification without density change.

B. Equilibrium for an open system

When the mass constraint is relaxed, the variational problem must refer to the functional [30],

$$\begin{aligned} \Omega &= \int [w'(\rho, \phi, T, \nabla\rho, \nabla\phi)] dv \\ &\equiv \int \left[w(\rho, \phi, T) + \frac{1}{2} \delta_F^2 (\nabla\rho)^2 + \frac{1}{2} \epsilon_F^2 (\nabla\phi)^2 \right] dv, \end{aligned} \quad (10)$$

where $w(\rho, \phi, T)$, is given by Eq. (4), and reduces to the grand canonical potential for the bulk phases in equilibrium. The corresponding Euler-Lagrange equations still read [see Eqs. (3)]

$$\frac{\partial w'}{\partial \rho} - \frac{\partial}{\partial x_i} \left(\frac{\partial w'}{\partial \rho_i} \right) = 0, \quad \frac{\partial w'}{\partial \phi} - \frac{\partial}{\partial x_i} \left(\frac{\partial w'}{\partial \phi_i} \right) = 0, \quad (11)$$

where ρ_i, ϕ_i indicate spatial derivatives with respect to the coordinate x_i . Here and in the following the summation convention over repeated indexes is used; an explicit dependence of the function w on its variables will be given later.

C. The capillary stress tensor

The equilibrium conditions (11) allow to find a general expression for the capillary stress tensor. Let us denote $\partial_i \equiv \partial/\partial x_i$, and calculate the gradient of the grand canonical potential density considering T as a constant parameter:

$$\partial_i w' = \left(\frac{\partial w'}{\partial \rho} \right) \rho_i + \left(\frac{\partial w'}{\partial \phi} \right) \phi_i + \left(\frac{\partial w'}{\partial \rho_k} \right) \rho_{ki} + \left(\frac{\partial w'}{\partial \phi_k} \right) \phi_{ki}. \quad (12)$$

Using the Euler-Lagrange equations (11) in Eq. (12) yields

$$\partial_i T_{ik} = 0, \quad (13)$$

where

$$\begin{aligned} T_{ik} &= \delta_{ik} w' - \rho_i \left(\frac{\partial w'}{\partial \rho_k} \right) - \phi_i \left(\frac{\partial w'}{\partial \phi_k} \right) \\ &= \delta_{ik} w' - \delta_F^2 \rho_i \rho_k - \epsilon_F^2 \phi_i \phi_k. \end{aligned} \quad (14)$$

Equation (13) states the mechanical equilibrium of the system, in terms of an intrinsically symmetric capillary tensor \mathbf{T} , where components are defined through Eq. (14) (δ_{ik} is the Kronecker symbol). Following the method indicated in [28] we show in the next section that \mathbf{T} represents the non-dissipative part of the overall stress tensor. An alternative form of Eq. (14) can be given observing that $w = -p + \rho(\partial w/\partial \rho)$ and using the first of Eqs. (3):

$$\begin{aligned} T_{ik} &= \delta_{ik} \left[-p + \rho \delta_F^2 \nabla^2 \rho + \frac{1}{2} \delta_F^2 (\nabla \rho)^2 + \frac{1}{2} \epsilon_F^2 (\nabla \phi)^2 \right] \\ &\quad - \delta_F^2 \rho_i \rho_k - \epsilon_F^2 \phi_i \phi_k, \end{aligned} \quad (15)$$

i.e., is in the diagonal part of \mathbf{T} the contribution due to the bulk pressure is clearly decoupled from the interface terms. In the case of a planar interface normal to z , Eq. (14) along with the Euler-Lagrange conditions yields

$$\begin{aligned} T_{zz} &= -P_0, \quad T_{xx} = T_{yy} = -P_0 + \delta_F^2 \rho_i \rho_k + \epsilon_F^2 \phi_i \phi_k, \\ T_{xz} &= T_{yz} = T_{xy} = 0, \end{aligned} \quad (16)$$

and the surface tension is given by

$$\gamma = \int_{-L}^{+L} (T_{xx} - T_{zz}) dz. \quad (17)$$

Thus we see that the difference between the stress normal to the interface and the tangential stress is the surface tension per unit length. This result is well known from the analysis of the equilibrium of fluid-fluid interfaces (see, for example [29]), and has been recovered here in a more general context.

To summarize, for a planar interface the equilibrium profile for the phase and density fields is governed by

$$\partial_z T_{zz} = 0; \quad \epsilon_F^2 \phi_{zz} - \left(\frac{\partial w}{\partial \phi} \right) = 0, \quad \left(\frac{\partial \rho}{\partial t} \right) = 0, \quad (18)$$

along with the condition of uniform and constant temperature. In the next section, we shall derive the dynamic equations for an out of equilibrium system.

III. THE DYNAMIC EQUATIONS

A. The entropy production rate

We now address the nonequilibrium situation through a thermodynamic procedure, starting from the local balance of mass, momentum, energy and entropy. Let us denote the velocity field by \vec{v} , the specific energy by e' , and the specific entropy by s' . The two latter quantities are determined by the specific free energy $f'(\rho, \phi, T, \nabla \rho, \nabla \phi)$ and in general involve gradient contributions. The stress tensor will be denoted by \mathbf{P} ; \vec{J}_E , \vec{J}_S stand for the energy and entropy flux vectors, respectively, and σ is the entropy production rate. Finally, \vec{g} stands for a specific body force field. In terms of these variables the classical balance laws read

$$\frac{d\rho}{dt} = -\rho \vec{\nabla} \cdot \vec{v}, \quad (19)$$

$$\rho \frac{d\vec{v}}{dt} = \rho \vec{g} - \vec{\nabla} \cdot \mathbf{P}, \quad (20)$$

$$\rho \frac{de'}{dt} = -\vec{\nabla} \cdot \vec{J}_E - \mathbf{P} : \vec{\nabla} \vec{v}, \quad (21)$$

$$\rho \frac{ds'}{dt} = -\vec{\nabla} \cdot \vec{J}_S + \sigma. \quad (22)$$

The constitutive relations and the explicit form of the fluxes will follow from the Courie principle and from the local form of the second law of thermodynamics, which implies $\sigma \geq 0$. In addressing the solid-liquid transition we will assume that the solid phase is at rest.

The specific Helmholtz free energy is given by

$$f'(\rho, \phi, T, \vec{\nabla} \rho, \vec{\nabla} \phi) = \frac{1}{\rho} \psi'(\rho, \phi, T, \vec{\nabla} \rho, \vec{\nabla} \phi) = f(\rho, \phi, T) + \frac{1}{2\rho} [\delta_F^2(\vec{\nabla} \rho)^2 + \epsilon_F^2(\vec{\nabla} \phi)^2], \quad (23)$$

where $f(\rho, \phi, T) = \psi(\rho, \phi, T)/\rho$ is the specific bulk free energy. The nongradient part of the specific energy and entropy are defined by

$$s(\rho, \phi, e) = -\frac{\partial f}{\partial T}; \quad e(\rho, \phi, s) = f(\rho, \phi, T) + T s(\rho, \phi, e). \quad (24)$$

Similar relations are postulated for the corresponding quantities incorporating gradient terms. Denoting

$$\delta_S^2 \equiv \frac{d\delta_F^2}{dT}; \quad \epsilon_S^2 \equiv \frac{d\epsilon_F^2}{dT}; \quad \delta_E^2 = \delta_F^2 - T \delta_S^2; \quad \epsilon_E^2 = \epsilon_F^2 - T \epsilon_S^2. \quad (25)$$

We obtain from Eq. (23)

$$s'(\rho, \phi, e, \vec{\nabla} \rho, \vec{\nabla} \phi) = s(\rho, \phi, e) - \frac{1}{2\rho} [\delta_S^2(\vec{\nabla} \rho)^2 + \epsilon_S^2(\vec{\nabla} \phi)^2], \quad (26)$$

$$e'(\rho, \phi, s, \vec{\nabla} \rho, \vec{\nabla} \phi) = e(\rho, \phi, s) + \frac{1}{2\rho} [\delta_E^2(\vec{\nabla} \rho)^2 + \epsilon_E^2(\vec{\nabla} \phi)^2]. \quad (27)$$

Under the above assumptions the differential form of the second law of thermodynamics reads

$$T ds' = de' - \frac{\partial f}{\partial \phi} d\phi - \frac{1}{\rho^2} \left[p - \frac{1}{2} \delta_F^2(\vec{\nabla} \rho)^2 - \frac{1}{2} \epsilon_F^2(\vec{\nabla} \phi)^2 \right] d\rho - \frac{1}{\rho} [\delta_F^2(\vec{\nabla} \rho) d(\vec{\nabla} \rho) + \epsilon_F^2(\vec{\nabla} \phi) d(\vec{\nabla} \phi)]. \quad (28)$$

Combining Eq. (28) with the balance equations (19),(20),(22) yields, after some manipulations,

$$\begin{aligned} \rho \frac{ds'}{dt} = & -\frac{\vec{\nabla} \cdot \vec{J}_E}{T} - \frac{\delta_F^2}{T} \vec{\nabla} \cdot \left(\frac{d\rho}{dt} \vec{\nabla} \rho \right) - \frac{\epsilon_F^2}{T} \vec{\nabla} \cdot \left(\frac{d\phi}{dt} \vec{\nabla} \phi \right) \\ & - \frac{1}{T} \frac{d\phi}{dt} \left(\rho \frac{\partial f}{\partial \phi} - \epsilon_F^2 \vec{\nabla}^2 \phi \right) - \frac{1}{T} (P_{ik} + T_{ik}) \partial_i v_k, \end{aligned} \quad (29)$$

where T_{ik} is the capillary stress tensor defined by Eq. (15) and rewritten, out of equilibrium, as

$$T_{ik} = \delta_{ik} \left(w' - \rho \frac{\delta \Omega}{\delta \rho} \right) - \delta_F^2 \rho_i \rho_k - \epsilon_F^2 \phi_i \phi_k. \quad (30)$$

We can rearrange Eq. (29) according to the entropy balance equation (22) adopting an entropy flux

$$\vec{J}_S = \frac{1}{T} \left[\vec{J}_E + \delta_F^2 \frac{d\rho}{dt} \vec{\nabla} \rho + \epsilon_F^2 \frac{d\phi}{dt} \vec{\nabla} \phi \right]. \quad (31)$$

Finally we find

$$\rho \frac{ds'}{dt} = -\vec{\nabla} \cdot \vec{J}_S + \sigma, \quad (32)$$

where the entropy production rate σ is given by

$$\begin{aligned} \sigma = & -\frac{1}{T} \frac{d\phi}{dt} \left(\rho \frac{\partial f}{\partial \phi} - \epsilon_F^2 \vec{\nabla}^2 \phi \right) + \vec{J}_E \cdot \vec{\nabla} \left(\frac{1}{T} \right) + \frac{d\rho}{dt} \vec{\nabla} \rho \cdot \vec{\nabla} \left(\frac{\delta_F^2}{T} \right) \\ & + \frac{d\phi}{dt} \vec{\nabla} \phi \cdot \vec{\nabla} \left(\frac{\epsilon_F^2}{T} \right) - \frac{1}{T} (\mathbf{P} + \mathbf{T}) : \nabla \vec{v}. \end{aligned} \quad (33)$$

As observed by Charach and Fife [31], the non classical contributions of the above equation (third and fourth terms on the right-hand side) can be treated, according to the Courier principle, as either of vectorial or of scalar origin, depending on the way in which the corresponding thermodynamic forces or fluxes are defined. However, to simplify the discussion, extending the choice of Wang *et al.* in their

model for solidification at constant density [12], we assume that $\epsilon_E^2 = \delta_E^2 = 0$; $\epsilon_S^2, \delta_S^2 = \text{const}$. Moreover in the sequel we shall neglect the spatial variation of both ϵ_F^2 and δ_F^2 , which amounts to neglect the thermal gradient across the interface. Then, the constraint of local positive entropy production reduces to

$$\frac{d\phi}{dt} = -\Gamma \left(\rho \frac{\partial f}{\partial \phi} - \epsilon_F^2 \vec{\nabla}^2 \phi \right), \quad (34)$$

$$\vec{J}_E = -K \vec{\nabla} T, \quad (35)$$

where Γ is a positive constant and K is the thermal conductivity. Moreover, assuming that the tensor contribution is only amenable to viscous dissipation, we obtain

$$\mathbf{P} = -\mathbf{T} - \mathbf{\Pi}, \quad (36)$$

with $\mathbf{\Pi}$ indicating the standard stress tensor for viscous fluids.

B. The grand canonical potential

We still need an explicit expression for the grand canonical potential density w . At equilibrium the latter is postulated as a double well over the ρ, ϕ plane, with two minima of equal depth centered at the bulk solid ($\rho = \rho_s, \phi = 0$) and liquid ($\rho = \rho_l, \phi = 1$). The undercooling of the system is described shifting the liquid branch through an additional term of the form $p(\phi)\rho\hat{L}(T_m - T)/T_m$, where \hat{L} is the heat of fusion per unit mass and T_m the pressure dependent melting temperature (in the sequel we shall use also a volumetric latent heat defined as $L = \rho_l\hat{L}$).

The function $p(\phi)$ is monotonic and increasing with ϕ , assuming the values $p(0) = 0, p(1) = 1$. We note that from a numerical perspective it is desirable to have fixed values of ϕ for the bulk phases. This result [which is incompatible with a linear dependence of $p(\phi)$] is obtained choosing $p(\phi) = \phi^3(10 - 15\phi + 6\phi^2)$.

In terms of a nondimensional density, scaled to the liquid density ρ_l , the following form for w revealed suitable for numerical calculations, retaining near the minima a paraboloid structure that should capture the essential physics of the problem:

$$w(\rho, \phi, T) = ag(\rho, \phi) + p(\phi)\rho\hat{L}\frac{(T_m - T)}{T_m}, \quad (37)$$

with

$$g(\rho, \phi) = \frac{1}{4}[\phi^2 + b(\rho - S)^2][(\phi - 1)^2 + b(\rho - 1)^2], \quad (38)$$

where $S = \rho_s/\rho_l$. The well height depends on the parameters a, b ; the latter fixes the stiffness of the potential in the ρ direction (i.e., the compressibility) with respect to the one in the ϕ direction. Notice that here and in the following we neglect thermal expansion effects and we assume equal compressibilities in both phases.

To complete the model, we must specify an equation of state relating the local pressure to the temperature and density fields. The latter takes the form

$$p = \rho \frac{\partial w(\rho, \phi, T)}{\partial \rho} - w(\rho, \phi, T). \quad (39)$$

Moreover, along a solid-liquid transition, the internal energy density \tilde{e} is assumed to change as

$$\tilde{e} = \tilde{e}_s + p(\phi)L. \quad (40)$$

Then, Eqs. (19)–(21), (34), and (39) along with specifications (35)–(37) and (40) and the Clapeyron equation, which accounts for the dynamical shift of the melting point, represent the evolution equations for the system.

C. Nondimensional equations in one dimension

We assume equal values of the thermal diffusivity D and the specific heat (at constant pressure) c_p in both phases. A nondimensional form of the model equations is obtained adopting a reference length ξ and scaling time to $\tau = \xi^2/D$. Density is scaled as ρ/ρ_l and a nondimensional temperature is introduced as $u = c_p(T - T_{m0})/L$, with T_{m0} being the initial melting temperature. The components of the stress tensor and the energy densities are scaled to $\rho_l v_0^2$, where $v_0 = \xi/\tau$ is the natural reference for velocities. Retaining for simplicity the same symbols for the scaled (nondimensional) quantities, and in absence of body forces, the model equations in one dimension read

$$\frac{\partial \rho}{\partial t} + v \frac{\partial \rho}{\partial z} = -\rho \frac{\partial v}{\partial z}, \quad (41)$$

$$\frac{\partial \phi}{\partial t} + v \frac{\partial \phi}{\partial z} = m \frac{\partial^2 \phi}{\partial z^2} - \frac{m}{\epsilon^2} \left[\frac{\partial g(\rho, \phi)}{\partial \phi} - p'(\phi)\rho \alpha \tilde{\epsilon}(u + u_D) \right], \quad (42)$$

$$\begin{aligned} \rho \frac{\partial v}{\partial t} + \rho v \frac{\partial v}{\partial z} = & -\lambda_1 \rho \frac{\partial}{\partial z} \frac{\partial g(\rho, \phi)}{\partial \rho} + \lambda_2 \rho \frac{\partial^3 \rho}{\partial z^3} + \lambda_3 \frac{\partial^2 v}{\partial z^2} \\ & + \lambda_1 \left[\frac{\partial g(\rho, \phi)}{\partial \phi} - \tilde{\epsilon} \frac{\partial^2 \phi}{\partial z^2} \right] \frac{\partial \phi}{\partial z}, \end{aligned} \quad (43)$$

$$\frac{\partial u}{\partial t} + v \frac{\partial u}{\partial z} = -p'(\phi) \left(\frac{\partial \phi}{\partial t} + v \frac{\partial \phi}{\partial z} \right) + \frac{\partial^2 u}{\partial z^2} + \frac{\lambda_3}{\lambda_5} \left(\frac{\partial v}{\partial z} \right)^2, \quad (44)$$

along with the state equations for pressure and the dynamical shift u_D of the pressure dependent melting point:

$$\begin{aligned} p = \lambda_1 \left[\rho \frac{\partial g(\rho, \phi)}{\partial \rho} - g(\rho, \phi) \right]; \quad u_D \equiv & \frac{c_p [T_{m0} - T_m(p)]}{L} \\ = & \frac{1}{\alpha \tilde{\epsilon} \lambda_1} \frac{1 - S}{S} p. \end{aligned} \quad (45)$$

TABLE I. Values of the model parameters.

Parameter	Value
S	1.11
m	0.05
$\tilde{\epsilon}$	0.001
α	530
b	1.6
λ_1	3560
λ_2	3.56×10^{-3}
λ_3	1.05×10^{-1}
λ_5	4940

The parameters appearing in the above equations are defined as

$$m = \frac{\Gamma \epsilon_F^2 \tau}{\xi^2}, \quad \tilde{\epsilon}^2 = \frac{\epsilon_F^2}{a \xi^2}, \quad \alpha = \frac{L}{c_p T_{m0}} \frac{L}{\epsilon_F} \frac{\xi}{\sqrt{a}},$$

$$\lambda_1 = \frac{a}{\rho_l v_0^2}, \quad \lambda_2 = \frac{\delta_F^2 \rho_l}{\xi^2 v_0^2}, \quad \lambda_3 = \frac{\eta}{\tau \rho_l v_0^2}, \quad \lambda_5 = \frac{L}{\rho_l v_0^2}, \quad (46)$$

where η is the fluid viscosity. Notice that imposing $\rho = S = 1$ the model collapses on the classical phase-field description of the solidification of a pure substance. In this case (see for example [12,32]) the model parameters m , $\tilde{\epsilon}$, α , ϵ_F , and a can be related to the material properties through

$$m = \frac{\mu \sigma T_{m0}}{DL}, \quad \tilde{\epsilon} = \frac{h}{\xi}, \quad \alpha = \frac{\xi}{6\sqrt{2}d_0},$$

$$\epsilon_F^2 = 6\sqrt{2}\sigma h, \quad a = 6\sqrt{2} \frac{\sigma}{h}, \quad (47)$$

where h is the interface thickness, σ the surface tension, and $d_0 = (\sigma c T_{m0})/L^2$ the capillary length, μ is the kinetic undercooling coefficient that relates the interface undercooling to the interface velocity v_I through $v_I = \mu(T_{m0} - T)$. We assume that the above equations still represent a reasonable estimation of the model parameters in terms of the thermo-physical properties of the material. To estimate δ_F we assumed equal contributions of the gradient terms to the surface tension, i.e., $\epsilon_F^2 = \rho_l \delta_F^2$.

To conduct the numerical simulations we referred to the thermo-physical properties of Nickel. However, due to limitations of computational resources, and to render more tractable the numerical integration, a compressibility value has been chosen, resulting in a sound velocity that is an order of magnitude lower than the actual value. The interface thickness has been chosen as $h = 20 \times 10^{-8}$ cm. With a length scale $\xi = 2 \times 10^{-4}$ cm, the resulting values of the nondimensional model parameters are summarized in Table I.

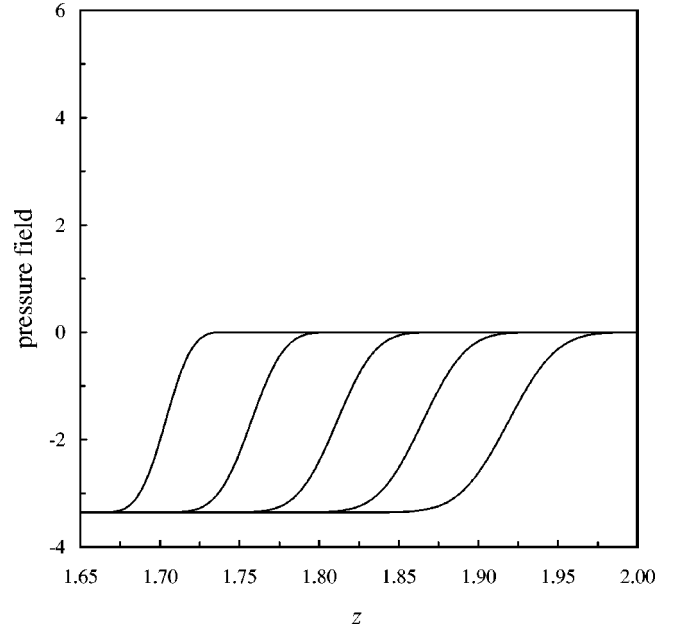


FIG. 1. The pressure wave originated at the solid-liquid interface. The interface is located near $z = 1.60$, and the different curves represent the pressure field at times 0.002, 0.003, 0.004, 0.005, and 0.006, from left to right. The wave speed is $v_s = 53.25$. The model parameters are specified in Table I.

IV. THE NUMERICAL METHOD

Equations (41)–(44) have been solved on the computational domain $0 \leq z \leq z_m$. Initially a phase boundary at $z = z_0$ separates a solid region ($z < z_0, \phi = 0, \rho = S$) from the liquid region ($z > z_0, \phi = 1, \rho = 1$). The system is initially at rest and the liquid is undercooled, i.e., $v(z, 0) = 0, u(z$

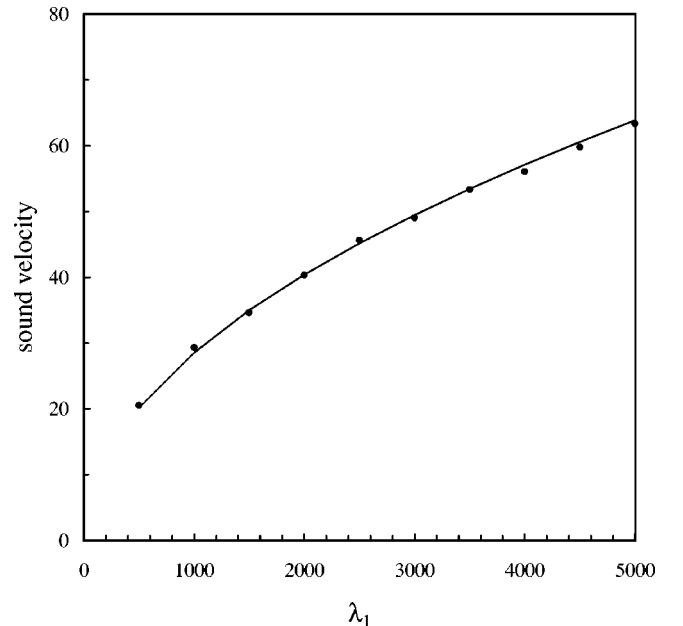


FIG. 2. The wave speed versus the slope λ_1 of the potential in the ρ and ϕ plane. The solid dots show the results of the present simulation. The line represents the theoretical prediction.

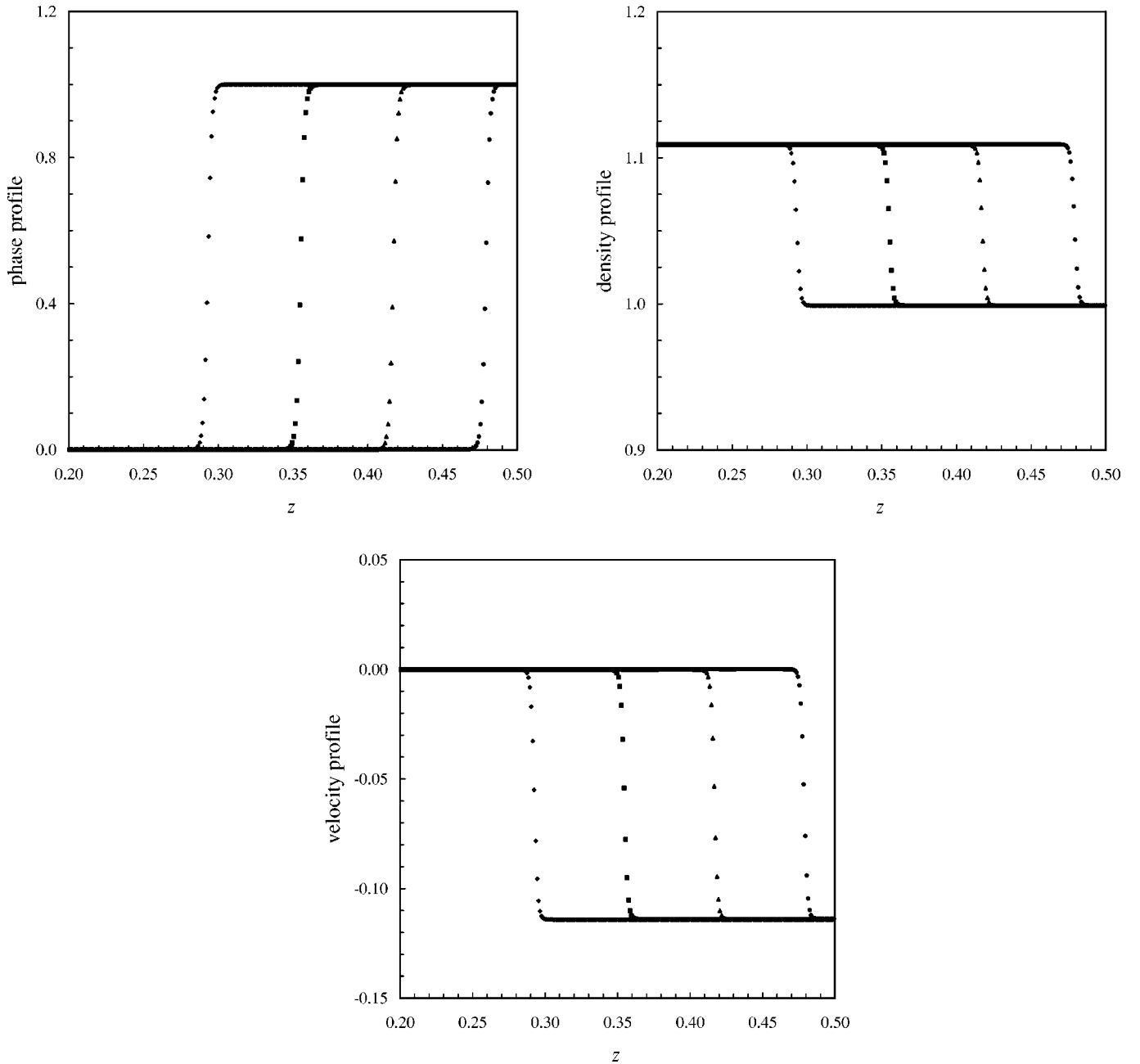


FIG. 3. The phase (a), density (b) and velocity (c) fields at different times. The curves are taken at $t=0.09$, $t=0.15$, $t=0.21$, and $t=0.27$ from left to right.

$\leq z_0, 0) = 0$, $u(z > z_0, 0) < 0$. For the phase, density, and temperature fields we imposed Neumann boundary conditions; the velocity is fixed as $v(0, t) = 0$ at the left end of the solid, while we chose $(\partial v / \partial z) = 0$ at $z = z_m$.

An explicit Euler integration scheme was employed to advance the solution forward in time. Second order central differences were used to discretize the Laplace operator, and upwind differences for the convective terms. To ensure an accurate resolution of the solid-liquid interface the grid spacing was selected as $\Delta z = \tilde{\epsilon}$; the time step required for numerical stability is $\Delta t = 0.4 \times 10^{-6}$. Following a standard method in computational fluid dynamics, the velocity field was

solved on a computational grid shifted of $\Delta z/2$ with respect to the one used for the scalar fields.

V. THE NUMERICAL RESULTS

We first checked whether the model gives a consistent description of the mechanical effects due to the density change in solidification. To this aim we solved the model equations at constant temperature ($u = -0.005$), fixing our attention to the mechanical relaxation of the system. The contraction of the liquid in front of the interface originates a pressure wave that propagates both into the solid and into the liquid. This effect is illustrated in Fig. 1, where only the liquid portion of the system is shown. The solid-liquid inter-

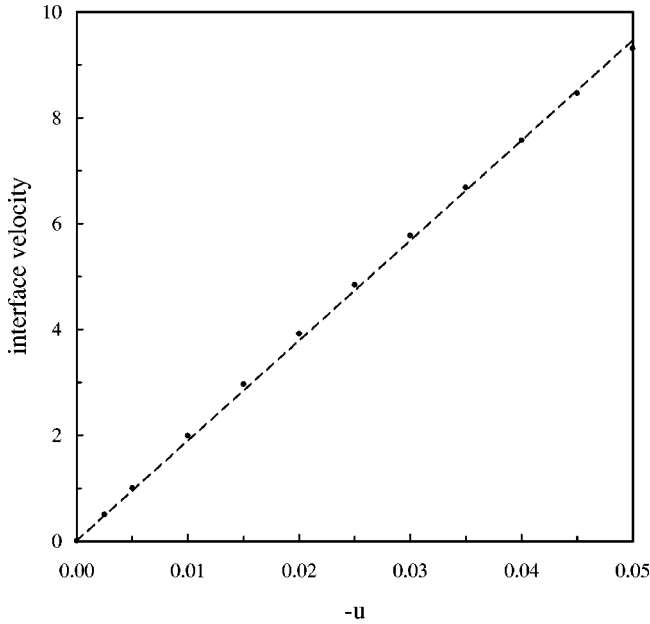


FIG. 4. The interface velocity versus the dimensionless undercooling of the melt (solid dots). The dashed line is the best fit of the numerical data. The model parameters are specified in Table I.

face is located near $z = 1.6$ (here and in the following all the numerical results will be presented in nondimensional form), and the pressure field is represented at different times. The initial pressure was initialized as $p(z,0) = 0$, and we see the negative pressure front that propagates into the liquid. The velocity of the wave, estimated tracking the position of the wave front, results $v_s = 53.25$; this value is in excellent agreement with the theoretical one for the liquid in equilibrium, ($\phi = 1, \rho_l = 1$), assumed as a pure elastic medium. The latter is $\sqrt{\partial p / \partial \rho} = \sqrt{0.5 \lambda_1 b [1 + b(1 - S)^2]} = 53.88$. To better characterize the process, we checked also the dependence of the wave speed on λ_1 . In Fig. 2 we show both the numerical results (solid dots) and the theoretical dependence $v_s(\lambda_1)$ (solid line). The agreement between the two sets of data (within 2%) is quite satisfactory. The small discrepancy is probably due to the dissipative behavior of our system.

After a short transient, growth at fixed temperature results in a steady advancement of the solid-liquid interface. In Figs. 3(a)–3(c) we show the phase, density, and velocity profiles obtained at different times, with $u = -0.005$. We observe that the solid is at rest, while the liquid is advected towards the interface with a velocity $v = -0.114$. The interface velocity, as resulting from the numerical data, is $v_I = 1.034$. Notice that this is the same value fixed by the mass conservation law through the relation $v = (1 - S)v_I$.

The growth of the solid phase into the liquid requires a departure from the local interfacial equilibrium. The classical phase-field model incorporates in a natural fashion this effect and, in the limit of a vanishingly small interface width, predicts a linear dependence of the growth rate on the interface undercooling. Caginalp and Jones [24] proposed a different interface relation, showing that in presence of fluid flow the front velocity in the kinetic undercooling term should be replaced by the front velocity minus the normal fluid veloc-

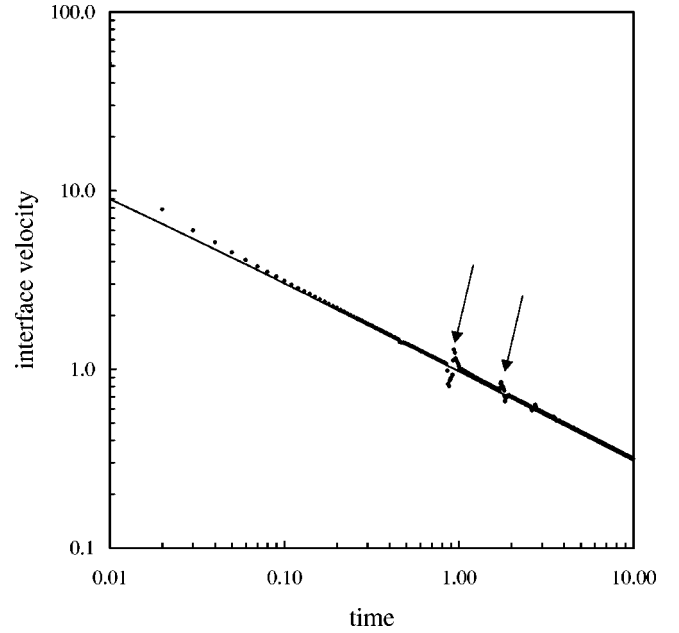


FIG. 5. The interface velocity as a function of time. The dimensionless undercooling is $\Delta = 0.75$. The solid line represents the diffusive solution obtained with $S = 1, b = 0$ (the classic phase-field model). The solid dots refer to the numerical solution of the present model. Notice the effect (indicated by the arrows) of the impact on the interface of the elastic wave reflected at the domain's walls.

ity. In steady growth, due to mass conservation, we still expect a linear behavior for the $v_I(u)$ dependence. This is confirmed by the results shown in Fig. 4, where we represent the growth rate versus the dimensionless undercooling. We observe that in the range represented in the figure, the data are well fitted by a straight line. As the interface velocity approaches the sound speed a different behavior should be expected, but this region is beyond the scope of the present study: for extremely high growth rates even the parabolic energy equation should be modified into a hyperbolic equation, to account for the finite speed of the thermal wave.

A central aim of our investigation was to check the effect of the convective heat transport on the dynamics of the growing interface. To this end we solved the full set of the model equations, allowing the thermal field to relax towards equilibrium. The initial undercooling was set as $\Delta = -u(z > z_0, 0) = 0.75$; to avoid finite size effects for the thermal field the domain's length was selected as $z_m = 25$. Figure 5 shows in a log-log plot the interface velocity versus time (solid dots). The arrows indicate the perturbation of the growth rate due to the pressure wave impinging on the interface, after the first and the second reflection on the domain's wall. In the same graph we represented the purely diffusive solution of the classic phase-field model (solid line), obtained by imposing $\rho = S = 1$. We observe that after a first transient the two sets of data converge towards the same asymptotic behavior: in either case the best fit of the data in the late stage of the growth ($t > 3$) indicates a power law $v \sim t^\alpha$, with α very close (within 0.15%) to the diffusional value $\alpha = -0.5$.

Then, at present the effect of the convective heat transfer

on the growth process seems to be negligible. However this point is far from being conclusive. Our analysis, performed in one dimension and for a planar geometry, discards interesting phenomena as the early growth of a spherical nucleus or the onset of morphological instabilities. Further investigation is required to assess the relevance of density effects for a more complex growth dynamics.

VI. CONCLUSIONS

The classical phase-field model is a well established tool to describe solidification far from equilibrium. In this paper we derived the governing equations of the model in the framework of the extended irreversible thermodynamics, considering different densities of the solid and liquid phases and taking into account the effects of capillary stresses. The equations reduce to the classical formulation for equal solid and liquid densities. The numerical solution of the model shows that the sound wave propagation, the interfacial dynamics, and the flow field are properly described.

We focused on the dynamical behavior of the growth pro-

cess for a dimensionless undercooling $\Delta = c(T_{m0} - T_\infty)/L < 1$, to investigate possible deviations from the purely diffusive picture. Our first results seem to indicate that in the late stage of the growth the process dynamics is almost unaffected by the density change effects. However, this point deserves further investigation. Our analysis was performed in one dimension and utilizes a planar geometry. Perhaps a more interesting behavior could be observed in a spherical geometry, due to the interplay between the capillary pressure and the dynamical shift of the equilibrium melting point. In the early stage of the process we observed the effects of the pressure wave originated at the solid-liquid interface. In our simulation the wave was redirected towards interface itself, after a reflection at the domain's walls. In a real process, as the nucleation starts, the homogeneity of the melt is rapidly lost and all the growing nuclei become the source of (primary or reflected) elastic waves. This phenomenon results in a new interaction mechanism between the growing germs, and could alter in a significant way the first stage of the crystal growth.

-
- [1] M. E. Glicksman, M. B. Koss, and E. A. Winsa, *Phys. Rev. Lett.* **73**, 573 (1994).
 - [2] G. P. Ivantsov, *Dokl. Akad. Nauk SSSR* **58**, 56 (1947).
 - [3] G. B. McFadden and S. R. Coriell, *J. Cryst. Growth* **74**, 507 (1986).
 - [4] V. Pines, A. Chait, and M. Zlatkowsky, *J. Cryst. Growth* **169**, 798 (1996).
 - [5] G. Horvay, *Int. J. Heat Mass Transf.* **8**, 195 (1965).
 - [6] Ch. Charach and I. Rubinstein, *J. Appl. Phys.* **71**, 1128 (1992).
 - [7] J. C. LaCombe, M. B. Koss, L. A. Tennenhouse, E. A. Winsa, and M. E. Glicksman, *J. Cryst. Growth* **194**, 143 (1998).
 - [8] G. Caginalp, *Arch. Ration. Mech. Anal.* **92**, 205 (1986).
 - [9] G. Caginalp, *Phys. Rev. A* **39**, 5887 (1989).
 - [10] G. Caginalp and P. Fife, *Phys. Rev. B* **33**, 7792 (1986).
 - [11] O. Penrose and P. C. Fife, *Physica D* **43**, 44 (1990).
 - [12] S. L. Wang, R. F. Sekerka, A. A. Wheeler, B. T. Murray, S. R. Coriell, R. J. Braun, and G. B. McFadden, *Physica D* **69**, 189 (1993).
 - [13] G. B. McFadden, A. A. Wheeler, R. J. Braun, and S. R. Coriell, *Phys. Rev. E* **48**, 2016 (1993).
 - [14] H. Lowen, J. Bechhofer, and L. Tuckerman, *Phys. Rev. A* **45**, 2399 (1992).
 - [15] A. A. Wheeler, B. T. Murray, and R. J. Schaefer, *Physica D* **66**, 243 (1993).
 - [16] G. Caginalp and J. Jones, *Ann. Phys. (Leipzig)* **237**, 66 (1995).
 - [17] G. Caginalp and W. Xie, *Phys. Rev. E* **48**, 1897 (1993).
 - [18] A. A. Wheeler, W. J. Boettinger, and G. B. McFadden, *Phys. Rev. E* **47**, 1893 (1993).
 - [19] M. Conti, *Phys. Rev. E* **56**, 3197 (1997).
 - [20] N. A. Ahmad, A. A. Wheeler, W. J. Boettinger, and G. B. McFadden, *Phys. Rev. E* **58**, 3436 (1998).
 - [21] Zhiqiang Bi and Robert F. Sekerka, *Physica* **261**, 95 (1998).
 - [22] M. Conti, *Phys. Rev. E* **58**, 6101 (1998).
 - [23] G. Caginalp and J. Jones, *Appl. Math. Lett.* **4**, 97 (1991).
 - [24] G. Caginalp and J. Jones, in *IMA Volumes on Mathematics and its Applications*, edited by M. E. Gurtin and G. B. McFadden (Springer, Berlin, 1991), pp. 29–50.
 - [25] D. W. Oxtoby and P. R. Harrowell, *J. Chem. Phys.* **96**, 3834 (1992).
 - [26] Ch. Charach (unpublished).
 - [27] L. K. Antanovskii, *Phys. Rev. E* **54**, 6285 (1996).
 - [28] D. M. Anderson, G. B. McFadden, and A. A. Wheeler, *Annu. Rev. Fluid Mech.* **30**, 139 (1998).
 - [29] A. J. M. Yang, P. D. Fleming III, and J. H. Gibbs, *J. Chem. Phys.* **64**, 3732 (1976).
 - [30] R. Evans, *Adv. Phys.* **28**, 143 (1979).
 - [31] Ch. Charach and P. C. Fife, *Open Syst. Inf. Dyn.* **5**, 99 (1998).
 - [32] J. A. Warren and W. J. Boettinger, *Acta Metall. Mater.* **43**, 689 (1995).